SCHLIEREN INTERFEROMETRY OF A PULSED GAS JET

SEMESTER THESIS

in Physics

Department of Physics

ETH Zurich

written by

BSc ETH PHYSICS
BENEDIKT HERMANN

supervised by

Dr. R. Tarkeshian
Dr. R. Ischebeck
Dr. A. Adelmann

May 25, 2016

Abstract

Within the scope of this Semester Thesis a complete setup for a Wollaston Prism Interferometer is built up and used to measure the atom density distribution of a conical Gas Jet (Argon and Xenon), that is pulsed by a piezo valve at a low repetition rate (3 Hz) with backing pressures ranging from 2 to 14 bar. Maximum densities of the order of $10^{17}\,\mathrm{cm}^{-3}$ (few mm away from the nozzle) are achievable with the Amsterdam piezo valve. The measurements show that the central density of the jet with Xenon is about 30 % lower than for Argon and the expansion angle of the Xenon jet is approximately 1.5° larger. The experiment can be used to characterize other gas jets (e.g. solenoid valves and different gases) or to study the density distribution when a blade is inserted into the gas flow, in order to shape and optimize the density distribution. This is of interest for an electron injection mechanism in Laser Wakefield Acceleration (LWA), which is based on a density ramp. Therefore, this study could be a base step towards a LWA design and implementation.

Contents

Chapter 1

Introduction and Theoretical Modelling

1.1 Schlieren Interferometry with Wollaston Prism

A Wollaston Prism consists of two crystals (e.g. quartz) which have a single optic axis. The axes of the two halves are rotated by 90 degrees. The main feature of these crystals is that the refraction index for light polarized parallel (n_e) to the optic axis is larger than for light polarized perpendicular (n_o) to the optic axis. Hence, a light ray polarized at 45° with respect to the optic axis will be split in two equally intense beams which have perpendicular polarization. The two rays will leave the prism at an angle ϵ, which depends on the geometric and optical properties of the crystals forming the Wollaston Prism. As exposed by Small [6],

$$\epsilon = 2\beta(n_e - n_o),$$

where β is the angle between the two halves of the (see Fig. 1.1). The Wollaston Prism used in this experiment manufactured by Societe d'Optique de Precision Fichou (Fresnes, France) has a dispersion angle of $20'' = 5.8$ mrad. If two light rays with an initial relative angle ϵ pass through the prism, the orthogonal part of the first ray will coincide with the perpendicular part of the second ray (compare Fig. 1.1). Before passing through the lens these two rays are separated by a distance $d = \epsilon f$. For the used Wollaston Prism and a lens with focal length f of 30 cm d is equal to 1.74 mm. If one places another polarizer at 45° after the prism, these two rays can interfere. This concept is illustrated in Fig. 1.1. Depending on the position of the prism relative to the focal point of the lens the interfering rays will pick up a phase difference. If the prism is centered at the focal point, every optical path runs equal distances through the two halves of the prism, i.e. no relative phase difference is generated. This scenario is called normal mode or infinite fringe width setup (IFW). Displacing the prism by a distance b from the focal point results in different path lengths of interfering rays and therefore these phase shifts leading to regular interference patterns on the screen. This setup is called differential mode or finite fringe setup (FFW) [2]. In that case the spacing S between the fringes is given by:

$$S = \frac{\lambda}{\epsilon}\frac{p}{b}$$

where p is the distance of the screen from the focal point of the lens [1]. The spacing can be decreased by increasing b, the position of the Wollaston Prism. If the screen is hold fix, p changes

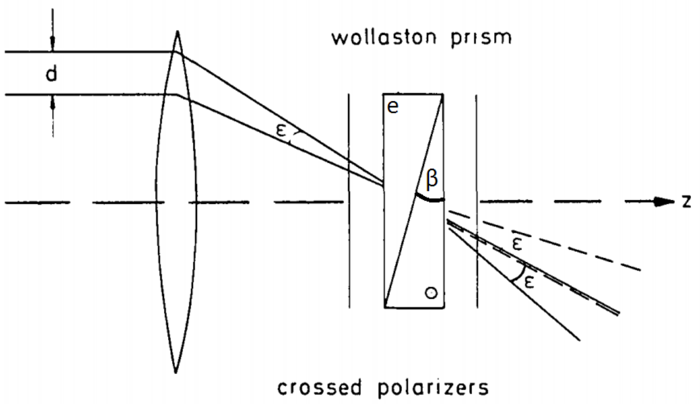

Figure 1.1: Working principle of the Wollaston Prism

accordingly. Placing a medium with refractive index $n \neq 1$ that covers only parts of the laser beam will result in a shift of the fringe spacing S, since rays passing through the medium will pick up a phase shift with respect to unperturbed rays (rays not traversing the medium).

1.2 Gas Density-Induced Phase Shift

A local density gradient imposes a varying refractive index n, resulting in a phase shift $\Delta\phi$ of rays passing through that particular region. Therefore, the undisturbed fringe spacing is locally shifted by ΔS. The relationship between the atom density ρ and refractive index n of a gas is given by the Lorentz-Lorenz equation

$$\rho = \frac{n^2 - 1}{n^2 + 2} \frac{N_A}{A} \approx (n - 1) \frac{2}{3} \frac{N_A}{A}, \tag{1.1}$$

where N_A is Avogadro‘s number and A is the molar refractivity, e.g. $A_{Xe} \approx 10.44 \times 10^{-6}$ m^3/mol. The approximation is valid for $n \approx 1$, which is true for a gas with densities in the order of 10^{18} particles/cm^3. Inverting Eq. 1.1 yields the dependency of the refractive index on the density. Assuming a homogeneous density within a gas jet of diameter l, the generated phase shift between interfering rays is approximately given by

$$\Delta\phi \approx l(n - 1) \frac{2\pi}{\lambda}. \tag{1.2}$$

Eq 1.2 represents an upper limit for the phase shift, since the used gas jet has a circular throat and hence, produces cylindrically symmetric jets, i.e. the length of a path through the gas is at most l. As described above, the fringe spacing is affected by the phase shift in the FFW setup; the fractional fringe distance shift is given by:

$$\frac{\Delta S}{S} = \frac{\Delta\phi}{2\pi}. \tag{1.3}$$

Figure 1.2 shows the phase shift calculated under the mentioned assumptions with Eq. 1.2 for a Xenon gas jet with a homogeneous density in the range of 10^{15} cm^{-3} to 10^{19} cm^{-3}. For

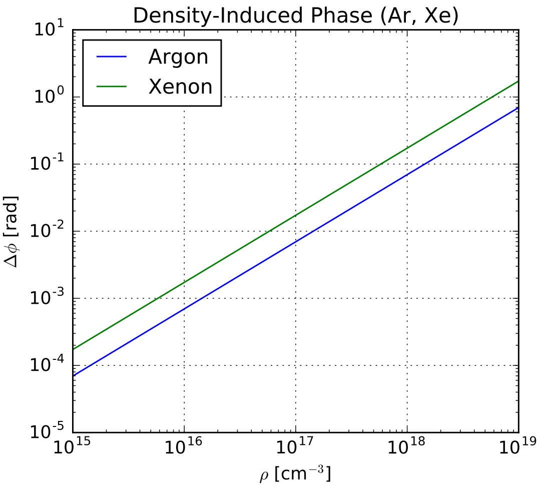

Figure 1.2: Estimation of phase shift induced by a gas distribution (Argon, Xenon) of length $l = 2\,\mathrm{mm}$ with homogeneous densities ranging from $10^{15}\,\mathrm{cm}^{-3}$ to $10^{19}\,\mathrm{cm}^{-3}$, $\lambda = 632.8$ nm.

that estimation the length of the gas jet was set to $l = 2\,\mathrm{mm}$, since the end of the nozzle is of comparable size (L=3.7 mm).

1.3 Density Estimation of a Conical Gas Jet

This section elaborates on the expected gas density of the piezo valve (Amsterdam Piezovalve, MassSpecpecD BV, Enschede, The Netherlands). The pressure of the gas before leaving the nozzle, called backing pressure, as well as the nozzle design play a crucial role for the density of the jet. The gas jet used in the present experiment has a conical nozzle with an half opening angle $\theta = 20°$ (see Fig. 1.3). As described in [3] the on axis particle density at position x of a conical gas jet is approximately given by

$$\frac{\rho}{\rho_0} = 0.15 \left(\frac{0.74d}{x \tan\theta} \right)^2, \tag{1.4}$$

where x as depicted in Figure 1.3, ρ_0 is the atom density of the gas before leaving the nozzle and d is the throat diameter of the valve. The gas jet used in this study has a throat diameter of $150\,\mathrm{\mu m}$, whereas L has a length of 3.7 mm. Therefore, x is basically equal the distance from the throat. Using the ideal gas law, that is a good assumption for Argon and Xenon, ρ_0 is determined by the so called backing pressure P_b which refers to the pressure in the chamber before the gas leaves the nozzle, as well as the temperature of the nozzle T_0 via: $\rho_0 = P_b/(k_B T_0)$ where k_B is the Boltzmann constant. Figure 1.4 shows the on-axis density n with respect to x for different backing pressures from 1 to 10 bar, an opening angle $\theta = 20°$, nozzle diameter $d = 150\,\mathrm{\mu m}$, and temperature $T_0 = 300$ K.

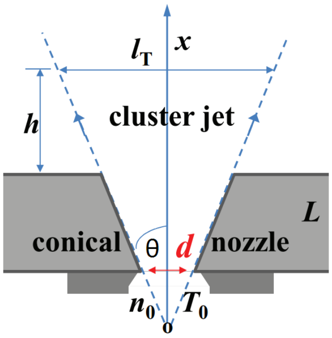

Figure 1.3: Sketch of a conical nozzle, taken from [3]. In the case of the used Amsterdam piezo valve x is roughly the distance to the throat, since $d \ll L$. $d = 150\,\mu\text{m}$, $L = 3.7$ mm, $\theta = 20°$.

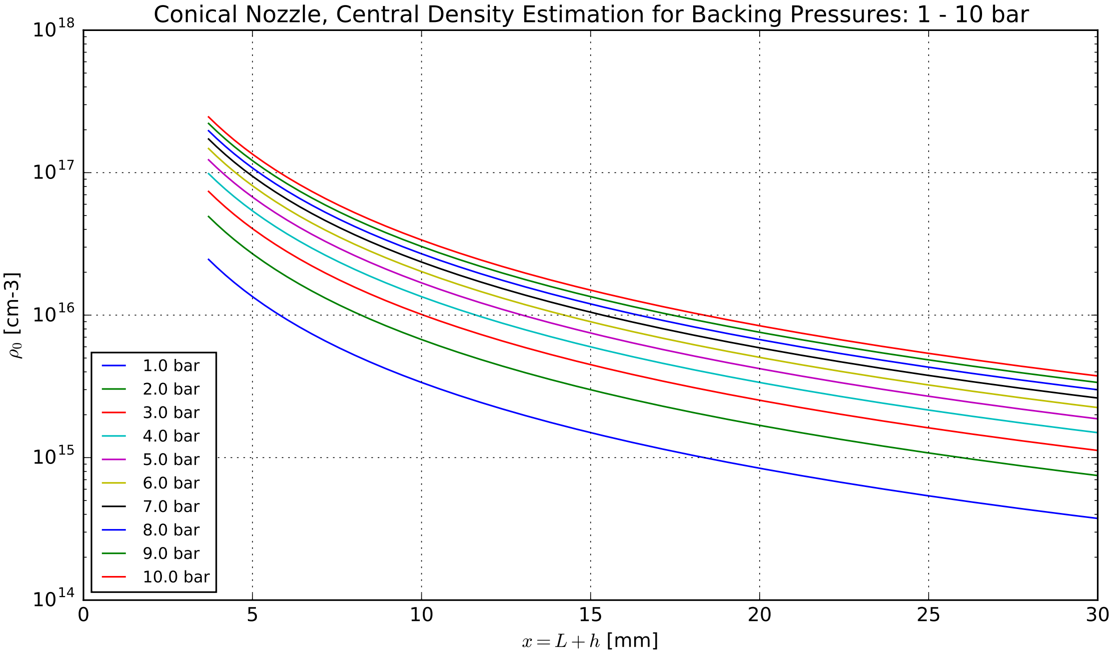

Figure 1.4: Estimation of the on-axis density ρ_0 for different backing pressures. This model is based on the ideal gas law, i.e. independent of the gas species.

Chapter 2

Experimental Setup

In Section 1.1 the working principle of the Wollaston Prism Interferometer has been explained. This chapter presents the experimental realization of this interferometer. Figs. **??** and 2.2 depict the experimental setup. A linearly polarized continuous He-Ne laser with a wavelength λ of 632.8 nm and an output power of 21 mW is used as a light source. The upstreaming air due to the heat of the laser causes a lot of unwanted phase shifts to the interference fringes. In order to shield the beam line from upstreaming air, a tilted black carton plate is placed above the laser. In order to minimize the airflow around the whole experiment, it is covered by a box made of the same black carton. The mutual laser diameter is 0.7 mm ($1/e^2$ width). The telescope (20x) attached to the laser provides a beam with a diameter of 14 mm, which is suitable to study a gas jet of a few millimeter. The noise of the acquired images is expected to be lowest in the center of the image due to the higher intensity of the laser there. The vacuum chamber has two facing broadband-anti-reflective windows to minimize light loss at these interfaces. The nozzle is hold by a stage (height adjustable) inside the vacuum chamber and the edge of the nozzle mount is used for calibration of distances in the image plane. The nozzle mount can been seen through the third window (see Fig. 2.3). The gas flows downwards, towards the vacuum pump (Pfeiffer HiCube Eco 80, 63 lit/s). The valve operates at 3 Hz and with opening times T less than 75 µs to reduce the gas load inside the chamber. The Wollaston Prism is placed between the two crossed polarizers, such that the interference fringes are parallel to the jet. The interference pattern is captured with a CCD camera (Basler Aviator avA2300-25gm) and a 200 mm Nikon camera lens. The minimal acquisition time of the camera is 18 µs. The acquisition time is set to 25 µs, in order to get an image with good contrast. The timing of the camera is shown in Fig. 2.4. The reference image (I1) is recorded 50 ms before the trigger signal T1 to the piezo controller. The second image I2 is recorded 25 µs after signal T1 such that the valve is completely opened during the total acquisition time. Since the valve operates at 3 Hz, 6 frames per second are acquired. Further Reduction of the time between I1 and T1 (50 ms) causes read out issues to the camera. The data processing of the obtained interference fringes is explained in the next chapter.

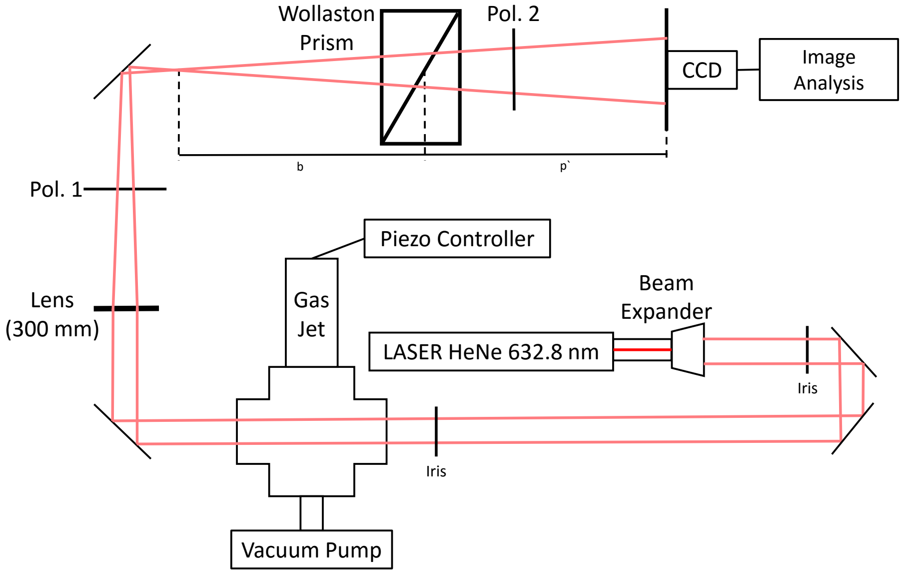

Figure 2.1: Sketch of the Experimental Setup.

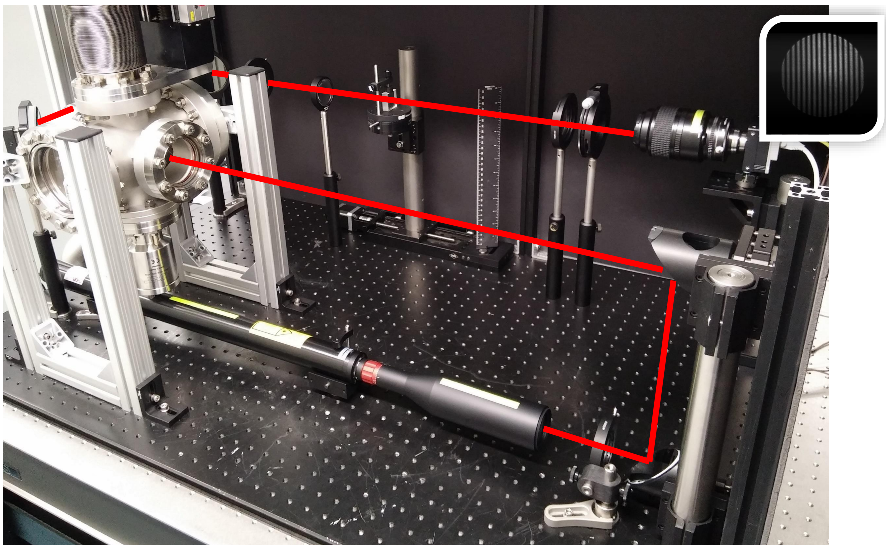

Figure 2.2: The He-Ne laser is placed below the vacuum chamber. The expander is attached directly to the laser. The expanded beam is brought to the height of the gas jet with two elliptical mirrors. After passing through the gas jet the expanded beam passes through the first polarizer, lens, Wollaston Prism, second polarizer and is projected onto the CCD screen via a 200 mm imaging lens.

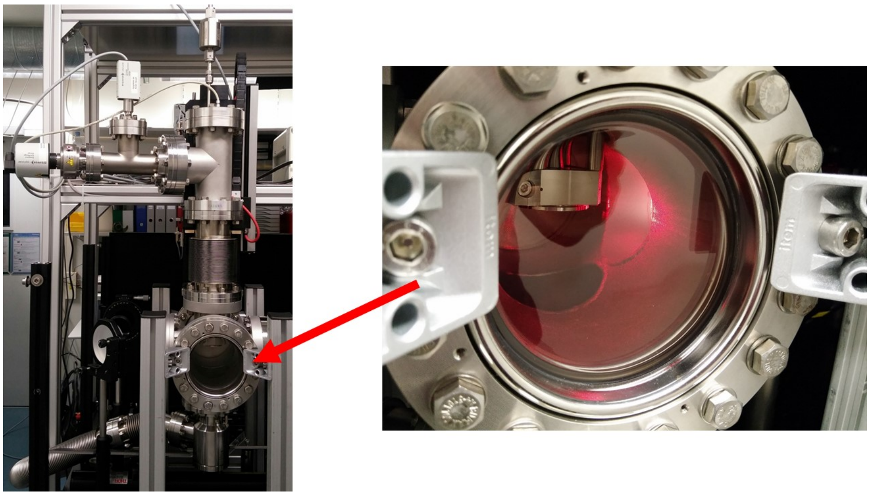

Figure 2.3: Adjustable nozzle mount.

```
10.0 GSa/s   1.00 Mpts
1 On ☑ 1.00 V/   2 On ☑ 500 mV/   3 On ☑ 1.00 V/   4 On ☐
H 10.0 µs/   38.0730000 µs   0   T 760 mV

Source       Vertical Scale  Offset     Horizontal Scale  Position
channel 1    1.00 V/div      1.000 V    10.0000 µs/div    38.0730000 µs
channel 2    500 mV/div      290 mV     10.0000 µs/div    38.0730000 µs
channel 3    1.00 V/div      2.320 V    10.0000 µs/div    38.0730000 µs
```

Figure 2.4: Screen shot of the oscilloscope: Purple: trigger for the first image (I1); Yellow: trigger for the second image with gas jet on (I2); Green: piezo controller output.

Chapter 3

Data Analysis

The expected phase shifts are of the order of 0.01 rad, as exposed in seciton 1.3. Fig. 3.1 shows the undisturbed interference fringes for Xenon at 6 bar backing pressure. A phase shift of $2\pi \times 0.01$ rad would mean that the fringe distance changes by one percent. This corresponds to a shift of roughly 0.1 mm on this printout. In order to reduce statistical noise of the CCD sensor, an average over 1000 images with jet on and off is taken instead of analyzing 2 single shots. Furthermore a Gaussian-weighted average along the gas flow direction (x) is taken. The Gaussian window has a length of 63 pixel (500 µm). This procedure is applied to 40 horizontal and equidistant lines for x between 4 mm and 12.7 mm; these profiles are used for further analysis. In the next section the used algorithm to extract the phase from the horizontal profiles is described. Instructions to run the Python scripts can be found in the readme file which is stored together with the scripts and data on the HDD of the experiment.

3.1 Phase Unwrapping based on FFT

The following phase extraction problem must be considered. Given noisy discrete values of a function of the form

$$g(y) = b(y) \cdot e^{\mathrm{i}[2\pi f y + \alpha(y)]}, \tag{3.1}$$

find $\alpha(y)$.

The term $b(y)$ takes global intensity changes into account, y is the coordinate perpendicular to the gas flow, f is the undisturbed oscillation frequency of the fringes and α represents the phase shift induced by the gas jet. This problem can be solved by fitting of the measured data to an Ansatz for $\alpha(y)$. This is not very appropriate, since one has to make (possibly incorrect) assumptions about the form of $\alpha(y)$. A more elegant way to directly unwrap the phase from the noisy data makes use of the Fourier Transform. The following steps must be considered.

- **Fourier Transformation of** g

  $$\mathcal{F}(g)(\omega) = \int_{-\infty}^{+\infty} e^{-\mathrm{i}2\pi\omega y} \cdot b(y) \cdot e^{\mathrm{i}[2\pi f y + \alpha(y)]} \, \mathrm{d}y \tag{3.2}$$

  Since the acquired signal is real, the whole information is contained in the positive frequency domain. In this case the spectrum has two significant peaks in this domain. One at the fringe frequency f and another at zero due to the slowly varying intensity. More precisely, b behaves like a broad Gaussian; the $1/e^2$ width is larger than the length of the considered interval. A Gaussian window is applied to the spectrum to cut this peak off.

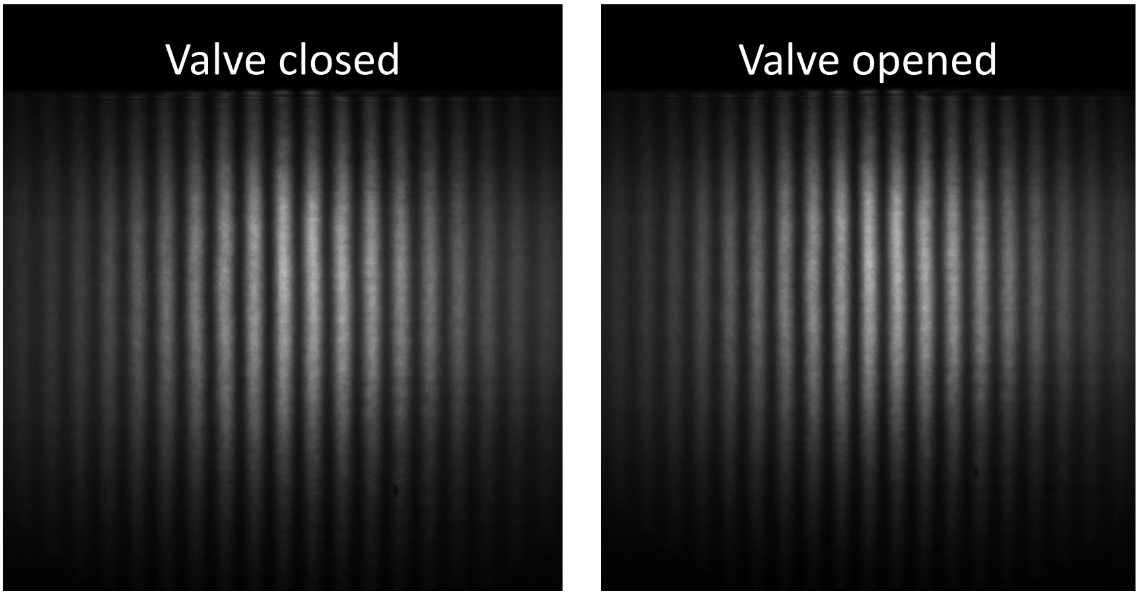

Figure 3.1: Interference fringes for Xenon at 6 bar backing pressure. The phase shifts are not visible by eye from the raw images. The gas flows vertical (x direction).

- **Rotation of the Fourier-transformed signal**

$$R_f\mathcal{F}(g)(\omega) = \mathcal{F}(g)(\omega + f) = \int_{-\infty}^{+\infty} e^{-\mathrm{i}2\pi\omega y} \cdot b'(y) \cdot e^{\mathrm{i}\alpha(y)}\, \mathrm{d}y \tag{3.3}$$

  The rotation by f shifts the peak at frequency f to zero. This eliminates the $2\pi f y$ phase factor. The purpose of this becomes obvious in the next step.

- **Inverse Fourier Transformation**

$$\mathcal{F}^{-1}(R_f\mathcal{F}(g))(y) = b'(y) \cdot e^{\mathrm{i}\alpha(y)} =: A(y) \tag{3.4}$$

  A contains the information about the phase shift α as well as remaining effects of b denoted by b'. These are minor effects due to imperfection at mirrors, lenses and polarizers or inhomogeneities of the two windows the laser passes through. These effects are eliminated by the next step.

- **$\mathbf{A/A_{ref}}$**
  Divide A by A_{ref} which is the array obtained by the same transformation applied to the reference signal without gas jet. What remains is an array of complex numbers who’s phase correspond to the phase caused by the gas jet.

As explained in section 1.1 the Wollaston Interferometer measures phase difference between positions separated by a distance d in the object plane. Therefore, phase shifts obtained at two points in the image plane that are separated by a distance corresponding to d have to be added up. The ideas behind the routine explained above come from the PhD thesis of Gilliss McNaughton Dyer [4], and are implemented as a Python script. The corresponding functions can be found in the Appendix 6.1. The explained procedure yields the phase ϕ which a ray has picked up when passing through the gas jet at the distance x from the throat, which is defined by the considered horizontal profile, i.e.

$$\phi(y) = \frac{2\pi}{\lambda} \int (n(y,z) - 1)\ \mathrm{d}z, \tag{3.5}$$

where the integration path goes along the ray through the jet, where λ is the wavelength of the laser and n refers to the refractive index of the gas. Once cylindrical symmetry of the gas distribution is assumed, obtaining the radial density distribution $\rho(r)$ from $\phi(y)$ is possible. The corresponding integral relation is called inverse Abel Transformation and is explained in the following section.

3.2 Error Analysis

A CCD sensor consists of an array of photo-diodes in which electrons are created by incident photons; the signal gets amplified and read out. This process of electron creation and multiplication is of statistical nature. Hence, the extracted phase profiles contain noise. The statistical noise can be suppressed by averaging over 1000 images. The standard deviation of the averaged signal is quantified locally by the following procedure: The phase signal for all of the 40 horizontal lines is smoothed by a Savitzgy-Golay filter with window size 51 pixel and polynomial order 3. The fitted curve is then subtracted from the original signal. The resulting data contains only noise. The standard deviation is taken at 25 equally large intervals, which is a compromise to get space resolved error estimation and to have large enough intervals to estimate the stadard deviation. The resulting noise map for Xenon at 6 bar backing pressure is plotted in Fig. 3.2. It is clearly visible that regions of high light intensity have less statistical noise. In the center of the laser beam the standard deviation of the signal is roughly 0.4 mrad, whereas 5 mm away from the center it is about 1 mrad. Xenon at 6 bar has a central phase shift of 30 mrad, 6 mm away from the nozzle, the standard deviation of the signal at that position is 0.5 mrad, i.e a very good signal to noise ration (SNR) of 60 is achieved (10 mm away from the nozzle a SNR of 20 is obtained). Therefore, the phase shift of the gas jet in the region of interest has been measured with sufficient precision in the region of interest.

3.3 Abel Inversion - From Phase to Radial Density

The phase shift ϕ extracted as explained above is a projection of the gas jet along the propagation direction of the laser. Cylindrical symmetry of the gas distribution is assumed. This enables to reconstruct the radial density distribution from ϕ. It is achieved by the inverse Abel transform. The Abel transform is nicely explained in [5] or [8].

$$\phi(y) = \frac{\Delta s}{\lambda} 2\pi = \frac{2\pi}{\lambda} 2 \int_0^\infty (n(y,z) - 1)\mathrm{d}z = \frac{4\pi}{\lambda} \int_y^\infty (n(r) - 1) \frac{r}{\sqrt{r^2 - y^2}} \mathrm{d}r \tag{3.6}$$

$$F(y) := \frac{\phi(y)\lambda}{2\pi} = 2 \int_y^\infty (n(r) - 1) \frac{r}{\sqrt{r^2 - y^2}} \mathrm{d}r \tag{3.7}$$

$$\overset{\text{inv. Abel}}{\Longrightarrow} (n(r) - 1) = -\frac{1}{\pi} \int_r^\infty \frac{\mathrm{d}F(y)}{\mathrm{d}y} \frac{\mathrm{d}y}{\sqrt{y^2 - r^2}} \tag{3.8}$$

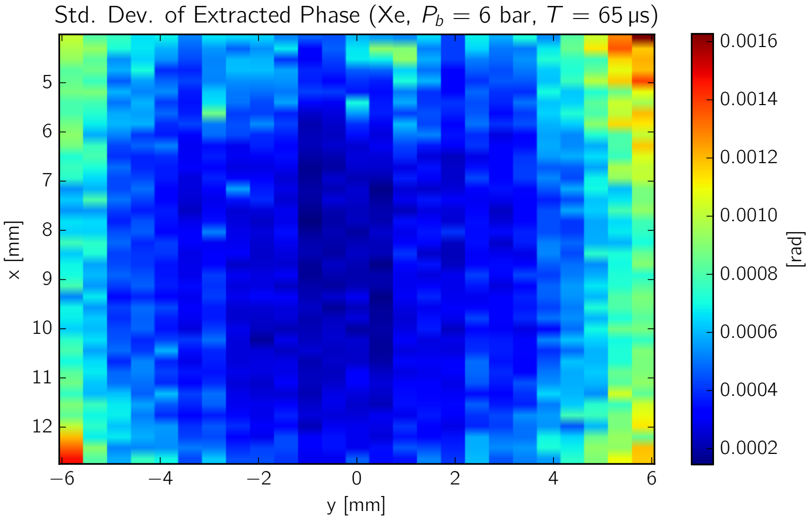

Figure 3.2: Standard Deviation of the Phase Shift Signal. The CCD sensor picks up less noise in regions of higher intensity, i.e. in the center of the laser beam.

The derivative and the integral occurring in equation 3.8 are calculated with the routines exposed by Joshua Stults [7]. The key points are summarised here. It is not possible to just approximate the derivative of F by the discrete differential quotient due to the noise, since that would amplify noise drastically. A more sophisticated method based on Gaussian filters is needed. Consider the following Fourier identity for f, g functions with compact support. All integrals appearing in equations 3.9 - 3.14 run from $-\infty$ to $+\infty$.

$$\mathcal{F}^{-1}\left[\mathcal{F}(f)\cdot\mathcal{F}\left(\frac{\mathrm{d}g}{dx}\right)\right] = \tag{3.9}$$

$$\mathcal{F}^{-1}\left[\int \mathrm{d}x\ e^{-\mathrm{i}2\pi x\omega} f(x)\cdot\int \mathrm{d}x\ e^{-\mathrm{i}2\pi x\omega}\frac{\mathrm{d}g(x)}{dx}\right] = \tag{3.10}$$

$$\mathcal{F}^{-1}\left[\int \mathrm{d}x\ e^{-\mathrm{i}2\pi x\omega} f(x)\cdot\int \mathrm{d}x\ e^{-\mathrm{i}2\pi x\omega}\ (\mathrm{i}2\pi\omega)\ g(x)\right] = \tag{3.11}$$

$$\mathcal{F}^{-1}\left[\int \mathrm{d}x\ e^{-\mathrm{i}2\pi x\omega}\ (\mathrm{i}2\pi\omega)\ f(x)\cdot\int \mathrm{d}x\ e^{-\mathrm{i}2\pi x\omega} g(x)\right] = \tag{3.12}$$

$$\mathcal{F}^{-1}\left[\int \mathrm{d}x\ e^{-\mathrm{i}2\pi x\omega}\frac{\mathrm{d}f(x)}{dx}\cdot\int \mathrm{d}x\ e^{-\mathrm{i}2\pi x\omega} g(x)\right] = \tag{3.13}$$

$$\mathcal{F}^{-1}\left[\mathcal{F}\left(\frac{\mathrm{d}f}{dx}\right)\cdot\mathcal{F}(g)\right] \tag{3.14}$$

If g is a Gaussian distribution, this identity gives a possibility to calculate the smoothed derivative of a signal f (equation 3.14) by using only the derivative of g instead of f (equation 3.9). The derivative of the Gaussian g can be easily evaluated from its analytical expression. Another issue is the singularity inside the integral of equation 3.8, when the integral is approximated on a discrete domain. This is solved by setting the first value of the integral ($y = r$) to the second value ($y = r + \Delta y$). For the limit of many points (i.e. small grid spacing Δy) the numerical value of the integral will converge to the analytical value [7]. The Python function performing these calculations can be found in the Appendix 6.1.

Chapter 4

Results

The numerical methods concerning phase extraction and inverse Abel transform are applied to the acquired data at 40 different distances measured from the throat. The length of the nozzle is $L = 3.7\,\text{mm}$. Therefore, the coordinate x starts at 4 mm of the density plots. The region closer to the throat cannot be measured (see Fig. 1.3). The field of view goes down to 12.7 mm, i.e. the spacing between two horizontal profile lines is 0.2 mm.

4.1 Density Distribution

Fig. 4.1 depicts the radial gas distribution for Xenon and Argon at 6 bar backing pressure with an opening time of 55 µs. From this image one can already see that the density for Xenon is roughly 30 % lower than for Argon, this is better seen in Fig. 4.2, which shows the radial density for selected distances from the throat (4.0 mm and 4.9 mm). The density is measured with opening time between 45 µs and 75 µs, but no significant dependency is observable. In Fig. 4.4 and 4.5 the central density for Argon and Xenon at different backing pressures is shown. The measured values of the central density agree up to a factor of 2 with the analytical model shown in Fig. 1.4. It is observed that the central density of Argon close to the nozzle does not increase much, when going beyond 11 bar. For Xenon this stagnation happens already at around 8 bar. Another relevant quantity of the gas jet is the Full-Width-Half-Maximum of the density distribution with respect to x (see Fig. 4.6). The FWHM of the Xenon jet is at the end of the nozzle slightly larger than for Argon under the same backing pressure. One can also see that the FWHM of the Xenon jet is growing faster. This becomes even clearer when considering the opening angle of the jet, which is shown in Fig. 4.7. The half opening angle γ is defined by the slope of the FWHM/2. For that purpose the data shown in Fig. 4.6 is fitted with a linear function by the numpy routine polyfit. From Fig. 4.7 one can infer that the expansion angle is increasing up to 11 bar. For even higher pressures the FWHM of Argon shows a decreasing behaviour, which can be explained by crystallising gas (clustering) in the following way. Initially the atoms have a certain random transverse momentum. When many atoms form a cluster the total transverse momentum is diminished.

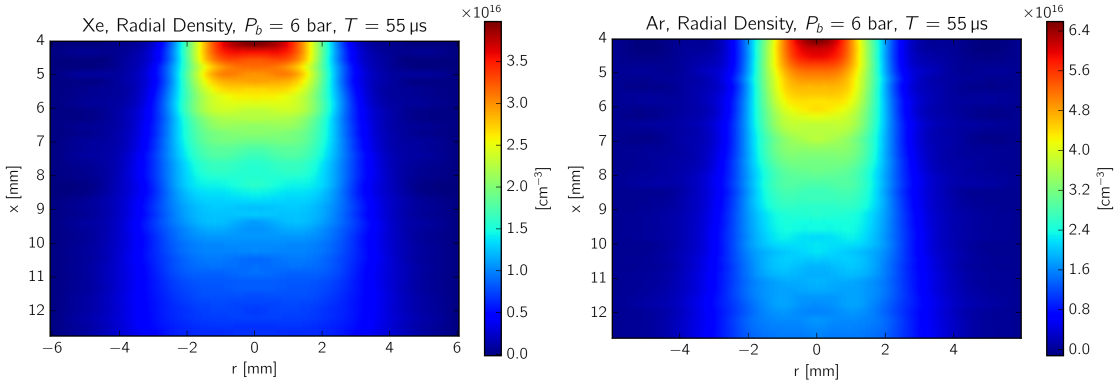

Figure 4.1: Map of radial density distribution of Argon and Xenon at 6 bar backing pressure and 55 µs opening time of the valve. The Argon jet has a higher absolute density and the distribution is narrower, for details consider the following Figures

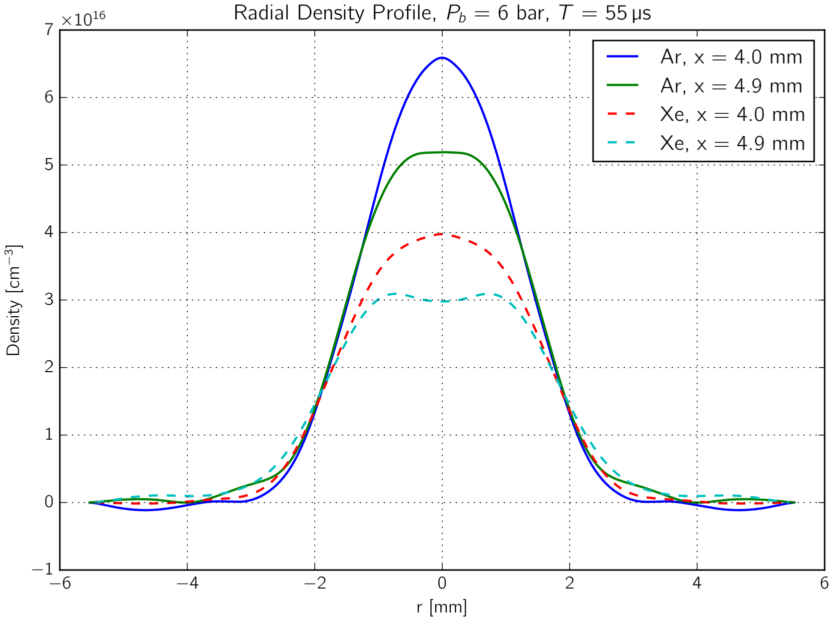

Figure 4.2: Radial density profiles at different distances from the throat for Argon and Xenon.

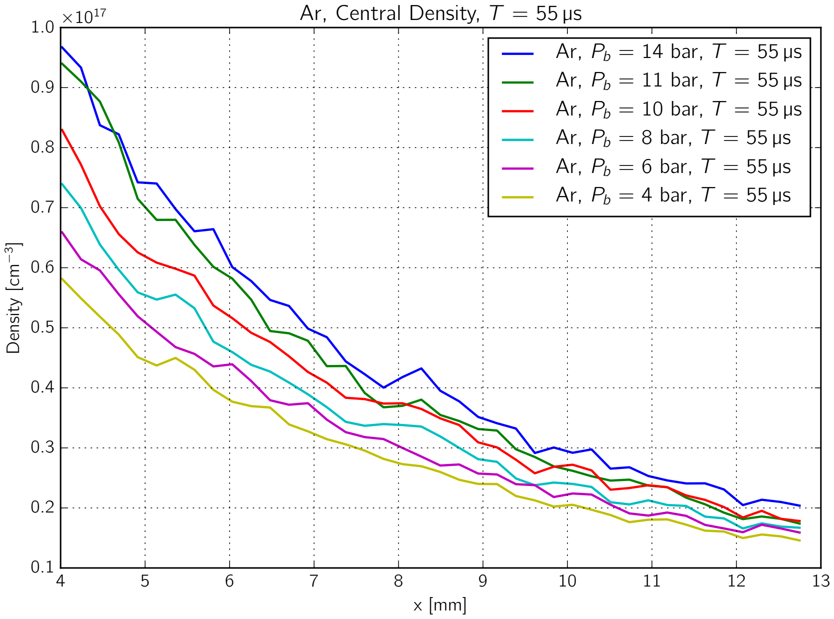

Figure 4.3: Central density of Argon at different backing pressures.

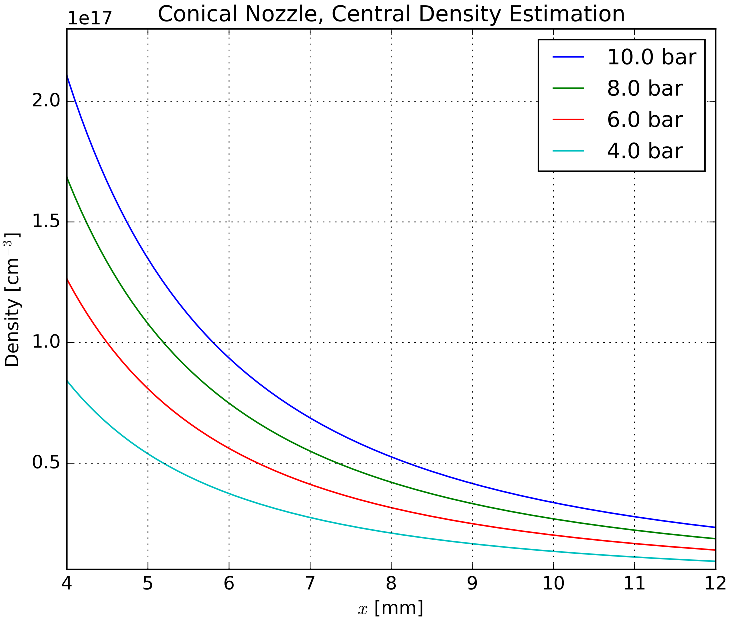

Figure 4.4: Analytical model of the central density of Argon at different backing pressures, explained in section 1.3

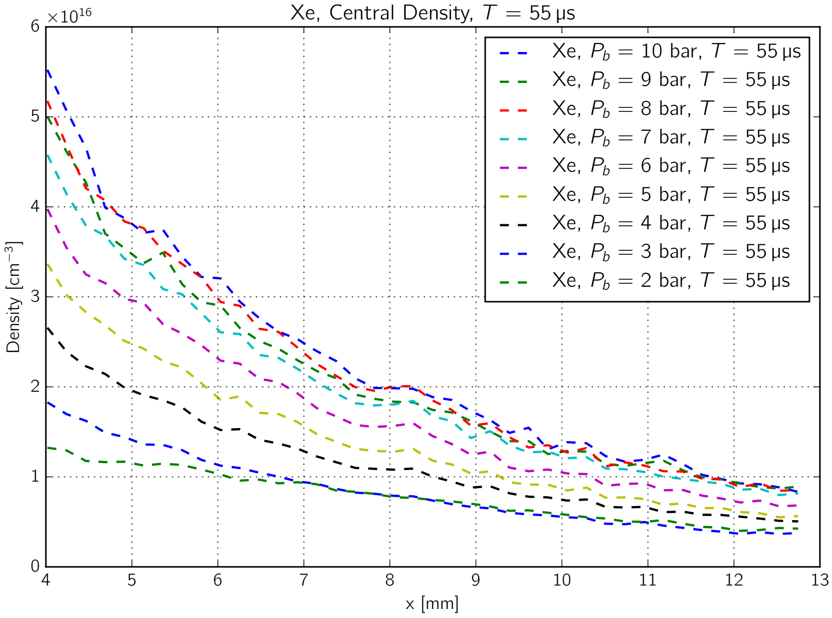

Figure 4.5: Central density of Xenon at different backing pressures.

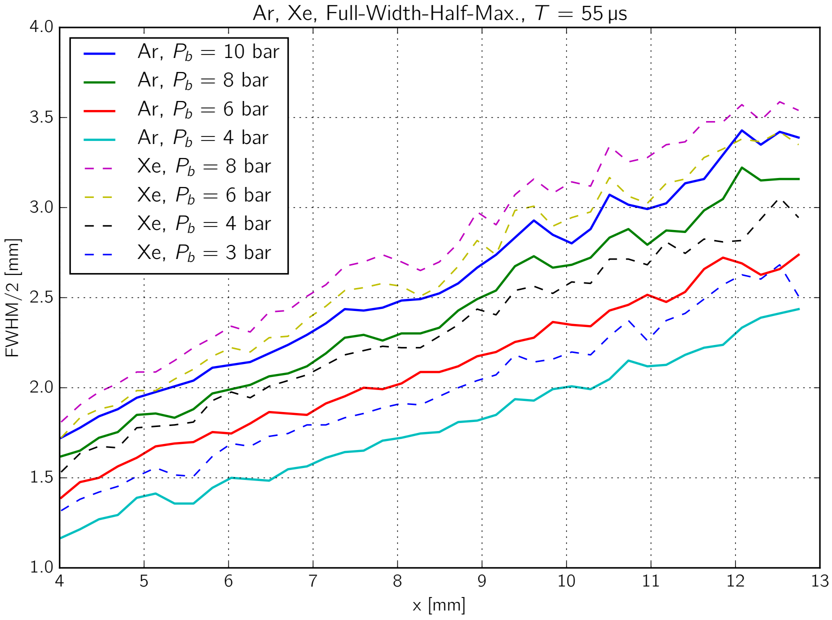

Figure 4.6: FWHM divided by 2 for Argon and Xenon at selected backing pressures.

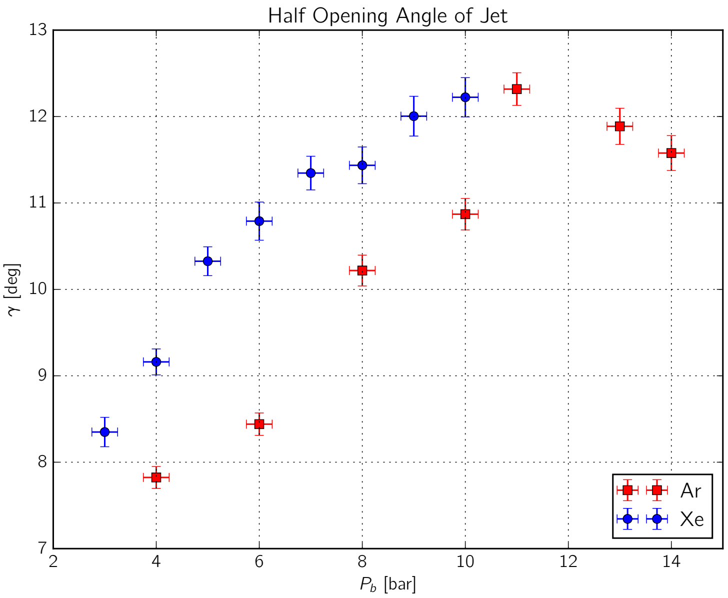

Figure 4.7: Half opening angle γ for Argon and Xenon with respect to backing pressure.

Chapter 5

Summary and Outlook

The atom density distributions of Argon and Xenon gas jets pulsed by the Amsterdam piezo valve have been measured. A maximum density of $10^{17}\,\mathrm{cm}^{-3}$, 1 mm apart from the nozzle, is obtained with the Argon jet. The maximum density of the Xenon jet is about 30 % lower. The FWHM right after the nozzle is roughly 3 mm and expands to 5 mm within 6 mm. The half opening angle (8° to 12°) depends on gas species and backing pressure and is 1.5° larger for Xenon compared to Argon. A stagnation of the opening angle at around 8 bar (Xe) and 10 bar (Ar) is observed.

The experimental setup can be used to characterize other valves (e.g. solenoid valves) or to study different gases. The setup may also be used for a laser Wakefield Acceleration (LWA) experiment for which a drastically higher gas density of the order of $10^{19}\,\mathrm{cm}^{-3}$ is needed. One possible electron injection mechanism is based on a density ramp which can by shaped by a blade that is inserted to the gas flow. The setup can be used to optimize the density distribution to enhance the electron injection in a LWA experiment. Since the rotational symmetry is broken by the blade, Abel inversion would not be applicable anymore. Hence, the density distribution must be reconstructed from many images taken from different directions.

Chapter 6

Appendix

6.1 Python Functions

The functions listed below are implemented in Python scripts that are stored on the HDD of the experiment. (Further information to use the scripts can be found in the readme file.)

Phase Unwrapping Algorithm

Input to the function phaseunwrap: (Z1, Z2)
One horizontal profile of the undisturbed fringes and one horizontal profile of the shifted fringes (jet on). It does not matter in which order Z1 and Z2 are inserted. The resulting minus sign is corrected at the end of the code. Z1, Z2 should be averaged over many (1000) images before, to reduce the noise of the CCD screen.
Output: Phase of Z1 w.r.t. Z2.

```
def phaseunwrap(Z1, Z2):
    """
    1. Fourier transform
    2. Gaussian window
    3. shift oszillation peak to zero
    3. inverse Fourier Transform -> A(x)
    4. A(x)/Aref(x)
    """
    #1 DFT
    N = len(Z1);a=0.;b=N
    t, step = np.linspace(a,b,N,endpoint=False,retstep=True)
    f = 1./N*(np.fft.fft(Z1))
    f2 = np.fft.fftshift(f)
    k = np.r_[-len(Z1)/2.:len(Z1)/2.]/(b-a)
    #2 Gaussian Window
    def Ga(x):
        return np.exp(-1./x**2*(3.*(k[1]-k[0]))**2)
    W1=(f2)*Ga(k)
    W1[0:len(W1)/2]=0
    #3 shift oszillation peak to zero
    b=np.argmax(W1)
```

```
    m=b-len(W1)/2
    S1=np.roll(W1,-m)

    D1=np.fft.ifft(N*S1)

    #same for ref. signal
    f = 1./N*(np.fft.fft(Z2))
    f2 = np.fft.fftshift(f)
    k = np.r_[-len(Z2)/2.:len(Z2)/2.]/(b-a)
    W2=(f2)*Ga(k)
    W2[0:len(W2)/2]=0
    m=np.argmax(W2)-len(W2)/2
    S2=np.roll(W2,-m)
    D2=np.fft.ifft(N*S2)

    #4 A(x)/Aref(x)
    E=D2/D1
    P1=np.zeros(len(S1))

    for i in xrange(len(S1)):
        P1[i]=cmath.phase(E[i])

    # minus sign if I1 and I2 are interchanged (gas on<-> gas off)
    if np.argmax(smooth(P1[len(P1)/10:-len(P1)/10]))<np.argmin(smooth(P1[len(P1)/10:-

    return P1
```

Abel Inversion Algorithm

Input to the function abel: (dfdx, x)
dfdx: Gradient of the projected density.
x: Coordinates in units of pixels; x=0 pix centered at the jet.
Output: Inverse Abel Transform of the density $\rho(r)$ calculated for both halves of the signal. If the gas jet is perfectly, rotationally symmetric both integrals are supposed to be equal up to noise.

```
def abel(dfdx, x):
    nx = len(x)
    integral = sp.zeros((2,nx/2), dtype=float)
    for i in xrange(nx/2, nx-1):
        divisor = sp.sqrt(x[i:nx]**2 - x[i]**2)
        integrand = dfdx[i:nx] / divisor
        integrand[0] = integrand[1] # deal with the singularity at x=r
        integral[0][i-nx/2] = - sp.trapz(integrand, x[i:nx]) / sp.pi
    for i in xrange(nx/2, 1, -1):
        divisor = sp.sqrt(x[i:0:-1]**2 - x[i]**2)
        integrand = dfdx[i:0:-1] / divisor
        integrand[0] = integrand[1] # deal with the singularity at x=r
        integral[1][-i+nx/2] = - sp.trapz(integrand, x[i:0:-1]) / sp.pi
```

```
    return(integral)
```

6.2 List of Main Parts of the Experiment

- Pizo Valve: Amsterdam Piezovalve, MassSpecpecD BV (Enschede, The Netherlands), throat: 150 µm, opening angle: 20°
- Piezo Controller: EDU1 Piezo Controller, Electronica Beta-VU, Amsterdam, The Netherlands
- Vacuum Pump: Pfeiffer HiCube Eco 80, $V = 63$ l/s
- Wollaston Prism: Societe d'Optique de Precision Fichou (Fresnes, France), 30x30x5 mm, $\epsilon = 5.8$ mrad
- 2 Linear Polarizers, 2 in diameter
- CCD Camera: Basler Aviator avA2300-25gm, 5 MP, min. acq. time: 18 µs
- Imaging Lens: AF Micro-Nikkor 200 mm f/4D IF-ED, Nikon
- Oscilloscope: Agilent infiniium DSA80000B, 3 GHz, 40 GSa/s
- Vacuum Gauge: Pfeiffer PKR 251 Full Range Gauge

6.3 Instructions to run the Experiment

Vacuum Pump

The chamber is pumped by Pfeiffer HiCube Eco 80 (PM S03 556 A) with a speed of 63 l/s. Operating the vacuum pump:

1. Press F1 to start the pre-pump.
2. Press F2 When reached pressure 100 mbar to switch on Turbo (turbo frequency goes up to 1500 Hz).
3. Switch off: Press F1 (Valve at the pump closes automatically).
   Note: The valve at the pump closes automatically when the pressure in the chamber increases by too much. That can be caused by long opening times or high piezo frequency.

Piezo Controller

Closing the valve:

1. Switch to pulsed mode.
2. Make sure no trigger signal is applied.
3. Apply piezo voltage of 148 V to 150 V.

Apply TTL trigger signal to piezo controller to open the valve. Set the desired opening time according to the pulse displayed on the oscilloscope. Use the 1:100 monitor output.

He-Ne Laser

1. Wear laser safety goggles! (He-Ne 632.8 nm)
2. Activate Interlock on the right side of the entry door. Laser safety light turns on and the laser is enabled to be powered.
3. Turn on laser with the key at High-Voltage supply.

Acknowledgements

First of all, I wish to express my gratitude to Andreas Adelmann for the organisation and motivating support. I also want to thank Rasmus Ischebeck and Roxana Tarkeshian for guiding and supervising the experiment with their professional experience. I wish to thank Hanspeter Gehrig for his support in the lab and many technical advices. I am indebted to Günther Dissertori for taking the initiative to make contact with Andreas Adelmann.
Finally, I am very grateful for the fruitful discussions about experimental, numerical and mathematical issues with my colleagues Peter Zenz and Nick Sauerwein.

Bibliography

[1] R. Benattar, C. Popovics, and R. Sigel. *Polarized light interferometer for laser fusion studies.* 1979. DOI: `http://dx.doi.org/10.1063/1.1135764`. URL: `http://scitation.aip.org/content/aip/journal/rsi/50/12/10.1063/1.1135764`.

[2] Matthew M. Biss et al. “Differential schlieren-interferometry with a simple adjustable Wollaston-like prism”. In: *Appl. Opt.* 47.3 (Jan. 2008), pp. 328–335. DOI: `10.1364/AO.47.000328`. URL: `http://ao.osa.org/abstract.cfm?URI=ao-47-3-328`.

[3] Guanglong Chen et al. “Understanding of cluster size deviation by measuring the dimensions of cluster jet from conical nozzles”. In: *AIP Advances* 3.3, 032133 (2013). DOI: `http://dx.doi.org/10.1063/1.4796187`. URL: `http://scitation.aip.org/content/aip/journal/adva/3/3/10.1063/1.4796187`.

[4] McNaughton Dyer Gilliss. “Experimental Study of the Equation of State of Isochorically Heated Warm Dense Matter”. PhD thesis. The University of Texas at Austin, UMI: 3274779, 2007.

[5] Simons Stephen N. and Yuan Zeng-Guang. “The Filtered Abel Transform and Its Application in Combustion Diagnostics”. In: *NASA Technical Reports* (2003). URL: `http://ntrs.nasa.gov/search.jsp?R=20030031381`.

[6] R. D. Small, V. A. Sernas, and R. H. Page. “Single Beam Schlieren Interferometer Using a Wollaston Prism”. In: *Appl. Opt.* 11.4 (Apr. 1972), pp. 858–862. DOI: `10.1364/AO.11.000858`. URL: `http://ao.osa.org/abstract.cfm?URI=ao-11-4-858`.

[7] Joshua Stults. *FFT-based Abel Inversion Tutorial.* Jan. 2010. URL: `http://www.variousconsequences.com/2010/01/fft-based-abel-inversion-tutorial.html`.

[8] Wikipedia. *Abel transform — Wikipedia, The Free Encyclopedia.* [Online; accessed 20-May-2016]. 2015. URL: `https://en.wikipedia.org/w/index.php?title=Abel_transform&oldid=668868856`.